Journal of Materials Chemistry A

Improved Stability and Efficiency of Perovskite/Organic Tandem Solar Cells with an All-inorganic Perovskite Layer

Journal:	*Journal of Materials Chemistry A*
Manuscript ID	TA-ART-12-2020-012286.R1
Article Type:	Paper
Date Submitted by the Author:	05-Mar-2021
Complete List of Authors:	Wu, Xin; City University of Hong Kong, CHEM Liu, Yizhe; City University of Hong Kong Qi, Feng; City University of Hong Kong, CHEM Lin, Francis; City University of Hong Kong, CHEM Fu, Huiting; City University of Hong Kong, Department of Materials Science and Engineering Jiang, Kui; City University of Hong Kong Wu, Shengfan; City University of Hong Kong, CHEM Bi, Leyu; City University of Hong Kong, Department of Chemistry Wang, Deng; City University of Hong Kong, Department of Materials Science and Engineering Xu, Fang; Shenzhen Technology University, Center for Advanced Material Diagnostic Technology Jen, Alex. K.-Y.; City University of Hong Kong Zhu, Zonglong; City University of Hong Kong, CHEM

ARTICLE

Improved Stability and Efficiency of Perovskite/Organic Tandem Solar Cells with an All-inorganic Perovskite Layer

Xin Wu,[a] Yizhe Liu,[a] Feng Qi,[a] Francis Lin,[a] Huiting Fu,[b] Kui Jiang,[b] Shengfan Wu,[a] Leyu Bi,[a] Deng Wang,[b] Fang Xu,[c] Alex. K.-Y. Jen[a,b] and Zonglong Zhu*[a]

All-inorganic perovskite solar cells (PVSCs) have attracted intensive attentions owing to their tunable bandgaps and excellent photo- and thermostability, making them as promising absorbers in tandem solar cells (TSCs). Herein, we develop an all-inorganic perovskite/organic TSC with a wide bandgap all-inorganic perovskite $CsPbI_{2.1}Br_{0.9}$ and a narrow bandgap organic photoactive layer (PM6:Y6) serving as top and bottom sub cells respectively. Fabricated tandem solar cell realized a remarkable PCE of 18.06 %, with an open-circuit voltage (V_{OC}) of 1.89 V, short-circuit current (J_{SC}) of 12.77 mA cm^{-2}, and fill factor (FF) of 74.81 %, which is higher than both the single junction PVSCs (14.43%) and organic solar cells (14.01%). Moreover, benefit from the outstanding UV and thermal stability of inorganic perovskites, the all-inorganic perovskite-based tandem devices showed superior stability under light and heat, with negligible degradation after 150 h of UV irradiation, 250 h under one sun illumination and 100 h heating at 80 °C, respectively. This work demonstrates that all-inorganic perovskite is an appropriate candidate for the fabrication of efficient and stable TSCs.

Received 00th January 20xx,
Accepted 00th January 20xx

DOI: 10.1039/x0xx00000x

1. Introduction

Metal halide perovskite solar cells (PVSCs), as one of the most promising photovoltaic (PV) technologies, have thrived expeditiously in the past decade by receiving a power conversion efficiency (PCE) over 25%.[1-5] Further commercialization of PVSCs requires considerately enhanced PCE and stability.[6] However, the Shockley-Queisser (S-Q) limit demonstrates the theoretical maximum PCE of single-junction PVSC can only achieve a value of 33.7% with 1.34 eV bandgap perovskite absorber.[7, 8] To break the S-Q limit, tandem solar cells (TSCs) have been developed to mitigate energy losses originating from thermalization of charge carriers.[9, 10]

Perovskite-based TSCs, which combines wide bandgap perovskites with narrow bandgap photoactive materials, such as silicon, copper indium gallium selenide ($Cu(In_xGa_{1-x})Se_2$, CIGS), have achieved high PCEs over 29%.[11-14] Although perovskite/Silicon and perovskite/CIGS tandem solar cells have achieved high performance, the cost of silicon and CIGS cells are relatively high due to expensive raw materials and energy-consuming fabrication process.[15] Moreover, the rigid nature of silicon films limits their application on flexible substrates.[16] As an alternate, perovskite/perovskite TSCs have appeared due to their low cost and compatibility for the fabrication of large-area flexible devices.[17, 18] Recently, considerable efforts on perovskite/perovskite TSCs have been made through optimizing the narrow bandgap Sn/Pb perovskite to achieve over 25% PCEs.[19, 20] However, several unignorable drawbacks still prohibit their development.[21, 22] Firstly, the Sn^{2+} in narrow bandgap perovskite can be easily oxidized to Sn^{4+}, further undermining the stability of tandem devices.[23] Secondly, high boiling point polar solvents (such as DMF and DMSO) are inevitably required when depositing narrow bandgap perovskite film.[24] Therefore, a compact and robust recombination layer (RL) must be designed fabricated to provide resistance against penetration of solvents.[25] To meet this demand, thermal sputtering or atomic layer deposition (ALD) is needed to prepare a transparent conductive oxide (TCO) or SnO_2 layer. However, the sputtering and ALD techniques rely on vacuum condition which leads additional energy-consuming process, not to mention gaining the complexity of device fabrication.

Apart from narrow bandgap perovskites, organic solar cells (OSCs) are widely employed to fabricate TSCs due to their tunable bandgap, high absorption coefficient, low-temperature solution-processed fabrication and compatibility with flexible substrates.[26-28] The hydrophobic property of organic layers with higher stability than Sn/Pb perovskites will be suitable to fabricate efficient and stable perovskite/organic TSCs.[29-34]

[a] *Department of Chemistry, City University of Hong Kong, Kowloon 999077, Hong Kong. Email: zonglzhu@cityu.edu.hk*
[b] *Department of Materials Science and Engineering, City University of Hong Kong, Kowloon 999077, Hong Kong.*
[c] *Center for Advanced Material Diagnostic Technology, College of Engineering Physics, Shenzhen Technology University, Shenzhen 518118, People's Republic of China.*

Electronic Supplementary Information (ESI) available: [details of any supplementary information available should be included here]. See DOI: 10.1039/x0xx00000x

Meanwhile, perovskite/organic tandem solar cells can be fabricated via solution process using orthogonal solvents, which has large potential for large-scale roll-to-roll production.[35-37] Therefore, perovskite/organic TSCs have been proved as a potential candidate to achieve stable and flexible solution-processed TSCs.[38] In order to realize long-term stability of perovskite/organic TSCs, all-inorganic perovskites demonstrate superior photostability and thermal stability than widely used organic-inorganic perovskite, which are much more promising candidates as sub cells for stable TSCs.[39] Recently, several groups have reported and reviewed the successful fabrication of all-inorganic perovskite/organic TSCs.[40, 41] For example, Lang *et al.* have fabricated perovskite/organic TSCs by employing $CsPbI_2Br$ and PTB7-Th:IEICO-4F as the top and bottom absorbers respectively, and achieved efficiency of 17.24%.[42] Xie *et al.* have achieved an efficiency of 18.38% by integrating $CsPbI_2Br$ with PM6:Y6 to construct tandem devices.[43] Although high efficiencies were reported, the stability of such devices haven't been studied, which requires systematical investigation.

In this work, a stable and efficient all-inorganic perovskite sub cell with 1.79 eV bandgap was developed by phenmethylammonium chloride (PMACl) passivation. The perovskite-organic tandem solar cells with a device configuration of ITO/SnO_2/$CsPbI_{2.1}Br_{0.9}$/PBDB-T/MoO_3/Ultrathin Ag/ZnO NPs/PM6:Y6/MoO_3/Ag was fabricated, which showed a power conversion efficiency (PCE) of 18.06 %, with an open-circuit voltage (V_{OC}) of 1.89 V, short-circuit current (J_{SC}) of 12.77 mA cm^{-2}, and fill factor (FF) of 74.81 %. Most importantly, as-prepared all-inorganic perovskite-based TSCs showed superior stability than the commonly used organic/inorganic hybrid perovskite-based devices, which has negligible degradation after 150 h of UV irradiation, 250 h under one sun illumination and 100 h heating at 80 °C. This work demonstrates that all-inorganic perovskite can be a promising candidate to fabricate efficient tandem cells with excellent long-term stability.

2. Results and Discussion

To develop highly efficient and stable perovskite/OSC TSCs, we firstly fabricated single-junction PVSCs with all-inorganic perovskite $CsPbI_{2.1}Br_{0.9}$. The perovskite was deposited according to our previous work.[44, 45] As the commonly used Spiro-OMeTAD is readily dissolved by the solution of PM6:Y6 in chloroform (CF) when depositing OSC sub cells, we replaced it with a polymer, PBDB-T, which is robust enough and keeps intact in the process of fabricating tandem devices due to its lower solubility in CF. The chemical structures of PM6, Y6 and PBDB-T are shown in Fig. S1. The configuration of perovskite single-junction cell was designed to be ITO/SnO_2/$CsPbI_{2.1}Br_{0.9}$/PBDB-T/MoO_3/Ag. Since the severe energy loss of this all-inorganic PVSC limits its performance, we employed phenmethylammonium chloride (PMACl) as a passivation agent to modify the surface of perovskite (Fig. 1a).

The current density-voltage (*J–V*) curves for the champion devices with (denoted as Cs-PMACl) and without PMACl (denoted as Cs-Ref) were shown in Fig. 1b, with the corresponding photovoltaics parameters summarized in Table S1. The Cs-Ref devices exhibited a champion PCE of 13.27 %, with V_{OC} of 1.07 V, J_{SC} of 15.40 mA cm^{-2}, and FF of 80.52 %. After treated with PMACl solution (2.5 mg mL^{-1}), the photovoltaic performance was improved to receive a champion PCE of 14.43 %, with a considerable V_{OC} of 1.15 V, J_{SC} of 15.46 mA cm^{-2} and FF of 81.19 %. The noticeably enhanced V_{OC} can be ascribed to the alleviated non-radiative recombination. The slightly strange shape of J-V curves for PBDB-T-based devices may be due to the unique charge transport properties of PBDB-T, similar results can be observed in previous literature.[46] The *J-V* curves of champion device with forward and reverse scan were shown in Fig. S2, which indicated a negligible hysteresis. The integrated J_{SC} determined from the EQE spectra were 14.82 and 14.87 mA cm^{-2} for the Cs-Ref and Cs-PMACl devices (Fig. S3), respectively, agreeing well with the value from *J-V* measurement. The relatively low EQE value in the range of 550 nm to 750 nm originates from the thin perovskite layer of 200 nm, which is designed for current matching in tandem device. Devices with Spiro-OMeTAD as hole-transporting material were also fabricated to confirm the effectiveness of PMACl passivation. As shown in Fig. S4, PMACl treatment results in an enhancement of V_{OC} from 1.07 V to 1.20 V. The *J-V* curves of devices treated with PMACl solution of different concentration (0 mg mL^{-1}, 1 mg mL^{-1}, 2.5 mg mL^{-1}, 5.0 mg mL^{-1}) were exhibited in Fig. S5 and Table S1. The concentration of 2.5 mg mL^{-1} resulted in the best performance, which is employed to fabricate single-junction and tandem devices hereafter.

To further study the mechanism of PMACl passivation, the UV-vis absorption, steady-state photoluminescence (PL) and time-resolved photoluminescence (TRPL) were measured**.** Fig. S6a showed the UV-vis absorbance spectra of Cs-Ref and Cs-PMACl perovskite film, which indicates that the PMACl treatment doesn't influence the absorption of perovskite film. The bandgap of as-prepared perovskite can be determined to be 1.79 eV (Fig. S6b). Fig. S7 exhibited the PL spectra of Cs-Ref and Cs-PMACl perovskite film, it is observed that the Cs-PMACl film showed obviously higher PL intensity than Cs-Ref film, suggesting the alleviated non-radiative recombination by PMACl passivation. What's more, a blueshift of PL peak from 689 nm to 684 nm can be noted, possibly due to the reduced shallow defects on the perovskite grain boundaries and surfaces.[47] The TRPL results in Fig. 1c and Table S2 demonstrated the average PL lifetime (τ_{ave}) of Cs-Ref and Cs-PMACl perovskite films to be 7.81 ns and 16.13 ns, respectively, confirming the alleviated non-radiative recombination via PMACl passivation.

Apart from the device performance, the stability of perovskites is also essential as large bandgap mixed halide perovskites tend to show phase segregation under continuous illumination. To test the stability, we firstly measured the PL and UV-vis spectra of perovskites with different composition before and after one sun illumination for different time. As shown in Fig. 1d, the PL peak of Cs-Ref perovskite film showed a slightly broadening, which was possibly attributed to the slight phase segregation. For the Cs-PMACl film (Fig. 1e), the PL peak remained unchanged and there is no broadening of peak after illuminated

for 60 min, indicating the Cs-PMACl perovskite is extremely stable without any phase segregation. This enhancement in stability may results from the suppression of halide migration.[48] The UV-vis absorption spectra in Fig. S8a, b showed the similar results, with PMACl passivated perovskite showed superior photostability.

To compare the photostability of all-inorganic perovskites with organic/inorganic hybrid perovskites for TSCs, we also measured the PL and UV-vis absorption spectra of organic/inorganic hybrid perovskite $FA_{0.8}Cs_{0.2}Pb(I_{0.6}Br_{0.4})_3$ (denoted as FACs) after illuminated for different time. FACs perovskite showed bandgap of 1.78 eV according to the measured absorption and Tauc plot (Fig. S9a, b). As shown in Fig. 1f, there is a notable red shift of PL peak after illuminated for more than 5 min, indicating the photo-induced phase segregation happened.[13] The PL intensity was also enhanced

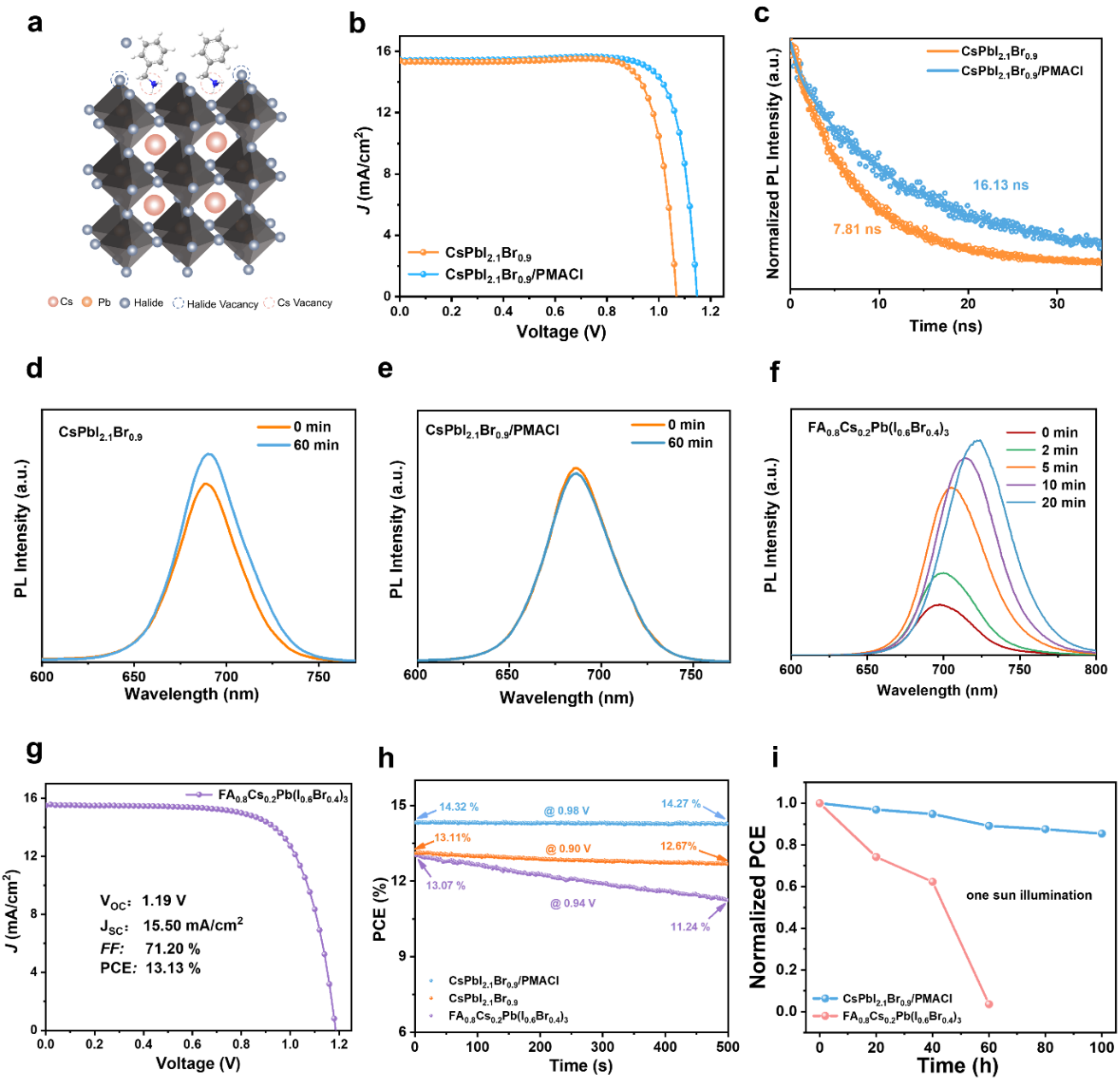

Fig. 1 (a) Schematic illustration of PMACl passivation; (b) Current density-voltage (J–V) curves of champion $CsPbI_{2.1}Br_{0.9}$-based device with and without PMACl passivation; (c) Time-resolved photoluminescence (TRPL) decay traces recorded from $CsPbI_{2.1}Br_{0.9}$ film and $CsPbI_{2.1}Br_{0.9}$/PMACl film; (d) Photoluminescence (PL) spectra of $CsPbI_{2.1}Br_{0.9}$ film before and after 60 min one sun illumination; (e) PL spectra of $CsPbI_{2.1}Br_{0.9}$/PMACl film before and after 60 min one sun illumination; (f) PL spectra of $FA_{0.8}Cs_{0.2}Pb(I_{0.6}Br_{0.4})_3$ film before after one sun illumination for different time (0, 2, 5, 10, 20 min); (g) J-V curve of champion $FA_{0.8}Cs_{0.2}Pb(I_{0.6}Br_{0.4})_3$-based device; (h) Stable output (SPO) at maximum power point (MPP) of champion $CsPbI_{2.1}Br_{0.9}$, $CsPbI_{2.1}Br_{0.9}$/PMACl and $FA_{0.8}Cs_{0.2}Pb(I_{0.6}Br_{0.4})_3$-based devices for 500 s; (i) PCE evolution of $CsPbI_{2.1}Br_{0.9}$/PMACl and $FA_{0.8}Cs_{0.2}Pb(I_{0.6}Br_{0.4})_3$-based devices under continuous one sun illumination for 100 h.

with a red shift, which has been reported before that the carriers tend to be concentrated into smaller bandgap emitters in multiphased perovskite film, leading to an increased local excitation intensity within small bandgap grains and resulting in high PL intensity in long-wavelength side.[49] Fig. S8c showed the change of absorption spectra of FACs perovskite under one sun illumination, the depletion of the ~670 nm absorption with simultaneous increase in the absorption at higher wavelengths also suggests the perovskite undergoes phase segregation.[49] Therefore, it can be concluded that all-inorganic perovskite had superior stability under illumination than FACs perovskite, which is a better choice for the fabrication of stable single junction and tandem devices.

Besides, we compared the stability of single-junction devices with different perovskite compositions. FACs-based devices were fabricated with the structure of ITO/SnO_2/$FA_{0.8}Cs_{0.2}Pb(I_{0.6}Br_{0.4})_3$/PBDB-T/$MoO_3$/Ag and showed a champion efficiency of 13.13 %, with V_{OC} of 1.19 V, J_{SC} of 15.50 mA cm^{-2}, and FF of 71.20 % (Fig. 1g, S9b), close to that of Cs-Ref device. The stable output (SPO) of champion Cs-Ref, Cs-PMACl, and FACs-based devices at the MPP under simulated one sun illumination were recorded (Fig. 1h). The Cs-PMACl device exhibited excellent stability with no obvious decay of efficiency for 500 seconds. Cs-Ref device showed slight degradation after 500-second illumination. In contrast, the FACs-based device showed poor stability, the efficiency decreased dramatically from 13.07 % to 11.24 % after illuminated for 500s. Meanwhile, Cs-PMACl and FACs-based devices were also set under continuous one sun illumination in a N_2 glove box for aging, Fig. 1i showed that Cs-PMACl based device retained over 85% of its initial efficiency after irradiated for 100 hours. In contrary, the efficiency of FACs-based device rapidly decayed after 60 hours. Hence, we can conclude that all-inorganic perovskite is appropriate for the fabrication of perovskite/OSC TSCs owing to the high performance and excellent intrinsic photostability.

Subsequently, we combined the 1.79-eV Cs-PMACl perovskite with ~1.30 eV narrow bandgap OSC (PM6:Y6) to fabricate

Table 1 The photovoltaic parameters of the all-inorganic perovskite top sub cell, OSC bottom sub cell, and 2T tandem solar cell under simulated AM 1.5G illumination.

	V_{OC} (V)	J_{SC} (mA cm^{-2})	FF (%)	PCE (%)
OSC	0.83	24.75	68.18	14.01
PVSC	1.15	15.46	81.19	14.43
Tandem	1.89	12.77	74.81	18.06
Average[a)]	1.89 ± 0.01	12.67 ± 0.08	71.53 % ± 1.92 %	17.17 ± 0.44 %

a) Averaged photovoltaic parameters from 30 tandem devices.

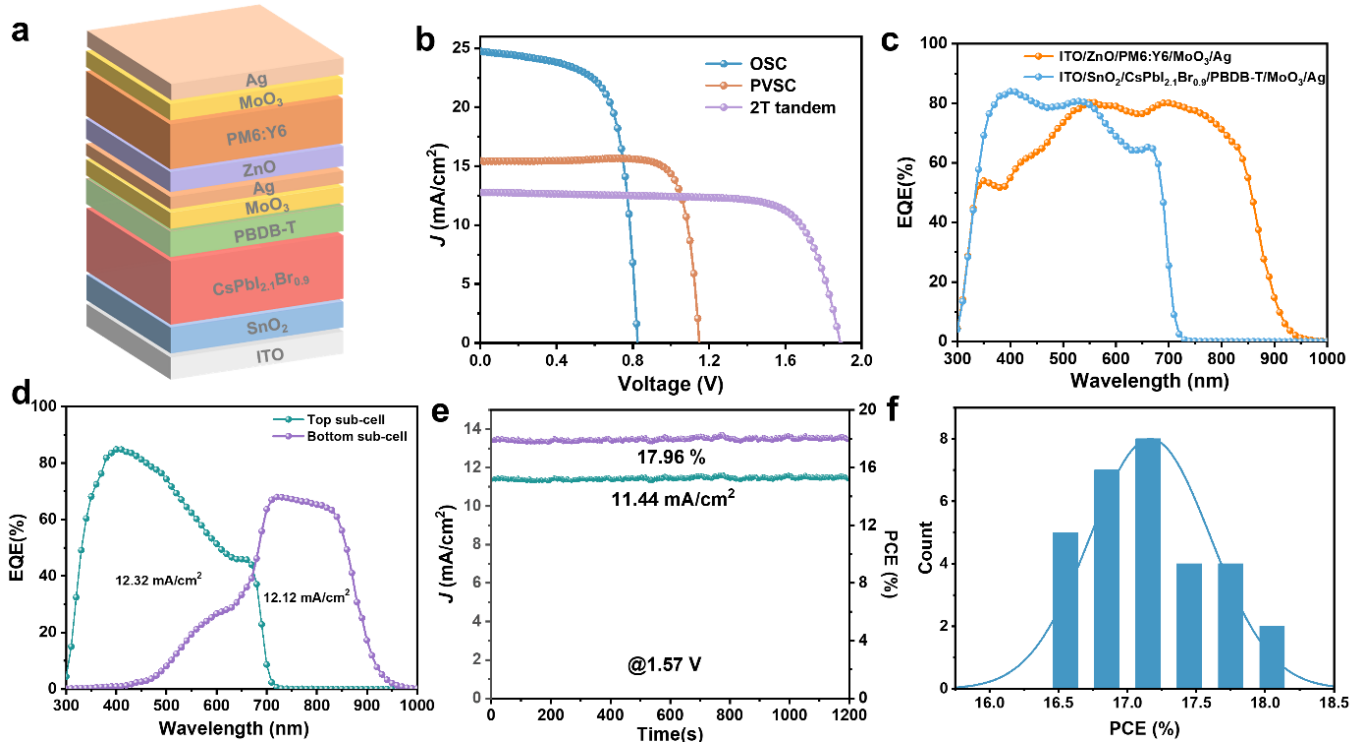

Fig. 2 (a) Schematic structure of the tandem device based on $CsPbI_{2.1}Br_{0.9}$ perovskite with PMACl passivation; (b) The *J–V* curves of single junction wide-bandgap PVSC, single-junction narrow-bandgap OSC, and 2T tandem solar cell under AM 1.5G illumination; (c) EQE spectra of single-junction wide-bandgap PVSC and narrow-bandgap OSC; (d) EQE spectra of wide bandgap perovskite top cell and narrow bandgap organic bottom cell, and the total EQE operating in the 2T tandem solar cell; (e) The stabilized output of a 2T tandem solar cell plotted as a function of continuous illumination time at the MPP condition with a steady bias voltage of 1.57 V; (f) The histograms of PCE of 2T tandem cells extracted from 30 devices.

tandem devices. Perovskite/OSC TSCs with the structure of ITO/SnO_2(20 nm)/$CsPbI_{2.1}Br_{0.9}$ (180 nm)/PMACl/PBDB-T (20 nm)/MoO_3 (6 nm)/Ag (1 nm)/ZnO NP (50 nm)/PM6:Y6 (110 nm)/MoO_3 (10 nm)/Ag (100 nm) (Fig. 2a) were designed and fabricated. One of the crucial issues for the fabrication of TSCs is to keep the underlayer films intact when depositing another layer. In this configuration, the ZnO nanoparticles were synthesized according to previous reports and dispersed in isopropanol (IPA),[50] which is an orthogonal solvent of perovskite. Meanwhile, the mixture of PM6:Y6 (1:1.2) was dissolved in chloroform (CF), which has low boiling point and evaporate rapidly after dripping, avoiding the damage to the underlayer robust PBDB-T. The cross-section SEM image in Fig. S10 confirmed the intact structure of fabricated tandem devices. To meet the requirement of current matching of two sub cells according to Kirchhoff's law, we tuned perovskite and interconnecting layer (ICL) with proper transparency. The transmittance spectra of ICL and the front cell/ICL were shown in Fig. S11a, b, respectively, which showed over 80% transmission in the near-infrared region, which guarantees the light absorption of organic bottom cell. Meanwhile, the ultra-thin 1 nm silver can effectively form ohmic contact with adjacent charge-selective layer for carrier recombination. Besides, the thickness of perovskite and PM6:Y6 were tuned to achieve current matching, Fig. S12 presented the *J–V* and EQE curves of TSCs with the thickness of PM6:Y6 ranging from 80 to 140 nm and the thickness of perovskite ranging from 110 to 250 nm, and the detailed photovoltaic parameters were summarized in Table S3, which showed that when the thickness of perovskite and PM6:Y6 are 180 nm and 110 nm respectively, the current matches. The *J–V* curves of the champion tandem devices and sub cells were plotted in Fig. 2b and corresponding photovoltaic parameters were summarized in Table 1. The single-junction OSCs showed a champion efficiency of 14.01%, with V_{OC} of 0.83 V, J_{SC} of 24.75 mA cm^{-2}, and FF of 68.18 %. The fabricated champion perovskite/organic tandem device showed a PCE of 18.06 % with V_{OC} of 1.89 V, J_{SC} of 12.77 mA cm^{-2}, and FF of 74.81 %. The high V_{OC} confirms the effectiveness of PMACl passivation and well-performed interconnecting layer. The increased FF of tandem devices than single-junction OSC may be attributed to the increased FF under lower light intensities due to the reduced carrier concentrations.[51] The champion tandem device exhibited a negligible hysteresis of *J–V* curves with forward and reverse scan (Fig. S13).

Fig. 2c showed the EQE of two single-junction sub cells, both the two sub cells showed considerable EQE value, with integrated J_{SC} of 14.87 mA cm^{-2}, and 23.57 mA cm^{-2}, respectively, consistent with the J_{SC} obtained from *J-V* measurement. The high EQE values are beneficial for the enhancement of light absorption in TSCs. Fig. 2d demonstrated the EQE spectra of the two sub cells operating in the tandem device, in which the two sub cells showed appropriate current matching with high EQE value

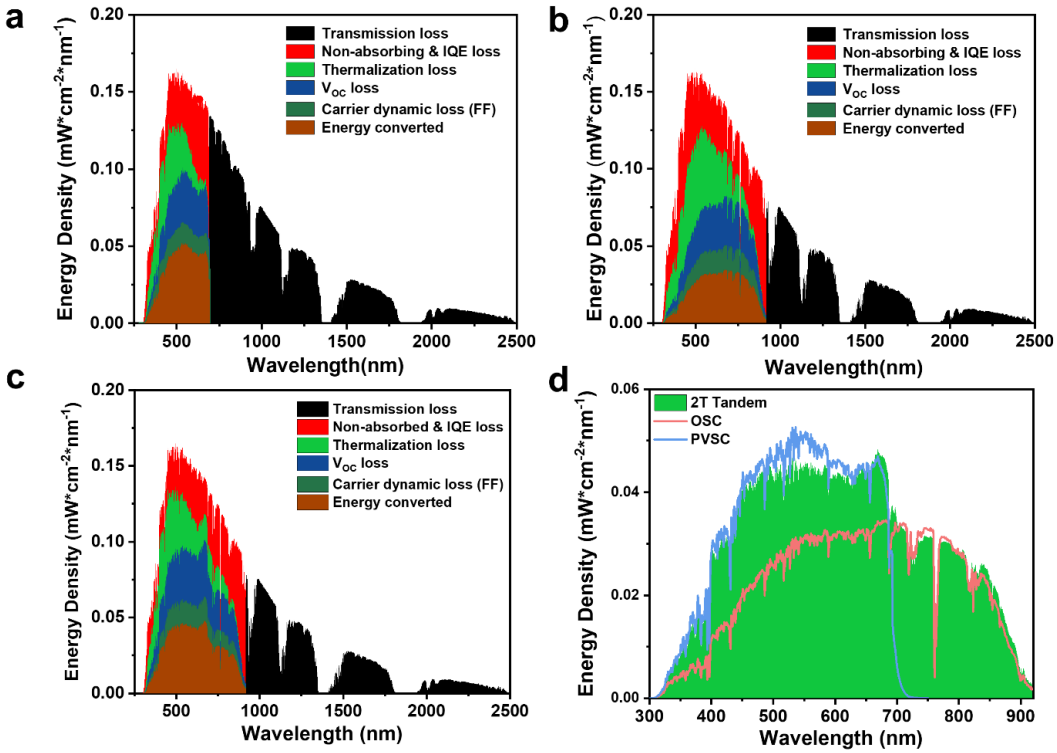

Fig. 3 Calculated energy loss for (a) single-junction PVSC, (b) single-junction OSC, and (c) 2T TSC. (d) Converted energy as a function of wavelength for single-junction device and tandem.

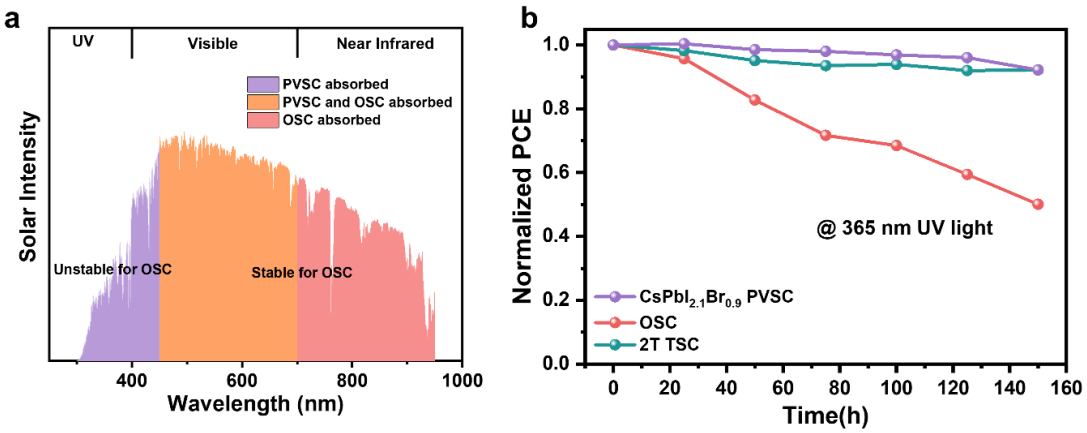

Fig. 4 (a) Schematic illustration of the filtering of UV light by perovskite top cell to protect the UV-unstable OSCs; (b) PCE evolution of single-junction $CsPbI_{2.1}Br_{0.9}$ PVSC, OSC and 2T tandem solar cells under 365 nm UV light.

between 300 nm and 950 nm. The integrated current densities of top and bottom cells are 12.32 mA cm^{-2} and 12.12 mA cm^{-2}, which is consistent with the J_{SC} obtained from *J-V* curves. The SPO of as-prepared TSC was also recorded at the MPP under simulated AM1.5G illumination for 1200 seconds, which exhibited a stabilized efficiency of 17.96 % (Fig. 2e) at the voltage of 1.57 V, demonstrating excellent stability under working condition. Fig. 2f showed the PCE statistics of 30 tandem devices, the efficiencies manifested normal distribution, indicating the excellent reproducibility of tandem devices. The statistical distribution of V_{OC}, J_{SC} and *FF* were shown in Fig. S14a, b, c, which also showed good reproducibility.

To gain deeper insight into the origin of device performance, we quantitatively analyzed the energy loss from sub cells and explained how the tandem structure improves device performance.[52] The energy loss analysis results of the single-junction PVSCs and OSCs are shown in Fig 3a, b, with corresponding energy loss values summarized in Table S3. As demonstrated, the transmission loss of perovskite single-junction cell (53.34 mW cm^{-2}) is significantly larger than that of OSC single-junction cell (30.44 mW cm^{-2}), which is due to its much larger bandgap and poorer coverage of solar spectrum. The large bandgap also results in much smaller thermalization loss in PVSC (8.47 mW cm^{-2}) than that in the OSC (15.93 mW cm^{-2}), as less photons with energy above the bandgap of perovskite are absorbed. Although the OSC shows smaller average *Voc,loss* than perovskite solar cells, the total converted energies of OSC (13.30 mW cm^{-2}) is still lower than that of PVSC (13.53 mW cm^{-2}), which is mainly attributed to the severe thermalization loss and insufficient light absorption. Therefore, balancing the transmission loss and thermalization loss is crucial for the enhancement of device performance in a solar cell. However, it remains difficult to simultaneously cut down the both losses in single-junction solar cells, as the bandgap of semiconducting material has already determined the pathways of both losses.

In the tandem structure (Fig. 3c, Table S4), the transmission loss is the same as in the OSC device due to identical absorption onset. However, the thermalization loss of tandem device is suppressed compared with single-junction OSCs. The total thermalization loss of tandem cell (12.46 mW cm^{-2}) is significantly reduced compared with OSC device (15.93 mW cm^{-2}) due to suppressed carrier thermalization. The larger total thermalization loss of tandem device than PVSC is attributed to the larger number of photons absorbed in tandem devices. To better compare the thermalization energy loss without the influences from absorbed photon number, the averaged thermalization loss per electron ($E_{therm}/N_{electrons}$) was introduced and calculated. The average E_{therm} of tandem device (0.51 eV) is obviously smaller than single-junction PVSC (0.57 eV) and OSC (0.68 eV), indicating the tandem structure can effectively alleviate the thermalization loss. Besides, the energy loss of tandem device caused by non-absorbed photons and IQE loss is also alleviated compared to OSC devices, perhaps due to the enhanced light absorption and improved total EQE. Fig. 3d depicted the wavelength dependent energy conversion, the tandem device showed improved efficiency due to the enhanced photo-response in the range of 300-700 nm and reduced thermalization due to the complementary light absorption. To conclude, the tandem structure efficiently balanced the transmission loss and thermalization loss, leading to improved device performance.

Moreover, the energy loss analysis also confirmed the great potential of perovskite/organic tandem structure to achieve higher performance than single-junction solar cells due to the simultaneously reduced transition loss and thermalization loss. The resultant imperfect efficiency of 18.06 % is mainly attributed to the severe $V_{OC,loss}$ and carrier dynamic loss caused by the two sub cells and interconnecting layer. Further reduction of $V_{OC,loss}$ of the two sub cells, developing wide-bandgap perovskites and narrow-bandgap organic absorbers with more well-matched light absorption, and continuous optimization of interconnecting layers will make it promising to achieve a PCE over 20%.

Stability is also an important issue for commercialization photovoltaic technology. As aforementioned, OSCs have been reported to be unstable under UV-light irradiation,[53] in contrast,

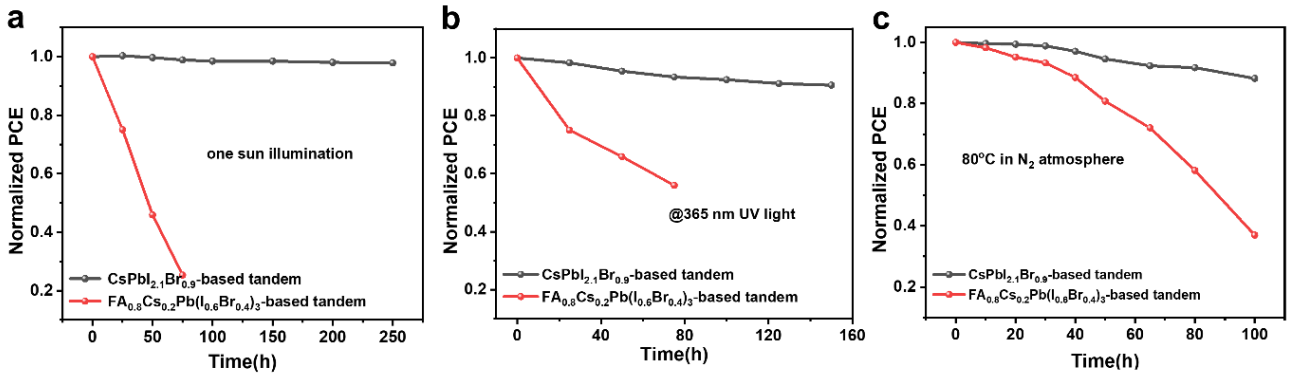

Fig. 5 PCE evolution of single-junction $CsPbI_{2.1}Br_{0.9}$-based tandem device and $FA_{0.8}Cs_{0.2}Pb(I_{0.6}Br_{0.4})_3$ based tandem device (a) under continuous one sun illumination, (b) under 365 nm UV light and (c) under 80°C heat in N_2 atmosphere.

all-inorganic PVSCs have demonstrated the most promising intrinsic stability under illumination. Fig. 1h has proved that all-inorganic PVSCs used in this work have superior stability under UV light, which is supposed to enhance the stability of the tandem device. The mechanism was depicted in Fig. 4a. In the tandem devices, the UV light was absorbed by all-inorganic perovskite front cell, protecting the OSC bottom cells from UV irradiation. As a result, the device became stable under UV light. To verify this hypothesis, we set fabricated all-inorganic PVSC, OSC, and TSC under 365 nm UV irradiation in a N_2 glovebox for aging. The devices were measured every 25 hours to record the efficiency evolution. As shown in Fig. 4b, the PCE of OSC device decayed rapidly to less than 50% of its original value after 150 hours. In contrary, the all-inorganic PVSC device and tandem device were quite stable and retained over 90 % of their original efficiencies, confirming that the all-inorganic PVSCs can act as a window to filter the UV light and contribute to a stable OSC-based TSC.

To contrast the stability of PVSC/OSC TSCs with different perovskite, we also fabricated tandem devices with FACs-based perovskite with the same configuration. Fig. S15 demonstrated the device structure, *J-V* curve of champion device and corresponding EQE spectra. The photovoltaics parameters are summarized in Table S5. The FACs-based TSCs showed a champion efficiency of 16.53%, with V_{OC} of 1.84 V, J_{SC} of 12.53 mA cm^{-2}, and FF of 71.72%, confirming the effectiveness of this tandem structure. As discussed in Fig. 1h, i, the $CsPbI_{2.1}Br_{0.9}$-based TSCs were supposed to show better stability than $FA_{0.8}Cs_{0.2}Pb(I_{0.6}Br_{0.4})_3$ based tandem device. We compared the stability of all-inorganic perovskite $CsPbI_{2.1}Br_{0.9}$-based tandem device (denoted Cs-TSC) with organic/inorganic hybrid $FA_{0.8}Cs_{0.2}Pb(I_{0.6}Br_{0.4})_3$ (denoted as FACs-TSC) (Fig. 5a, b, c). The Cs-TSCs showed superior stability to FACs-TSC under both 365 nm UV irradiation and one sun illumination, retaining over 90% of its initial PCEs after aging (Fig. 5a, b). In contrast, FACs-TSCs swiftly decayed to less than 60% of their original efficiencies, indicating all-inorganic perovskite-based TSCs have better photostability. Besides, as the all-inorganic perovskites are theoretically more stable than those with organic cations due to the volatile nature of organic cation, we also compared the thermal stability of Cs-TSC and FACs-TSC at 80 °C in N_2 atmosphere. As depicted in Fig. 5c, Cs-TSC retained over 85% of its initial PCE after heated at 80 °C for 100 hours. However, FACs-TSC demonstrated poor stability, the efficiency of FACs-TSC decreased to less than 50% of its original value after annealing for 100 hours. The stability results suggest that all-inorganic perovskites are better choice to fabricate stable tandem devices.

3. Experimental

3.1 Materials

The CsI was purchased from Sigma-Aldrich. PbI_2 and $PbBr_2$ are purchased from TCI. $HC(NH_2)_2I$ was obtained from Dyesol. PM6, Y6 and PBDB-T were purchased from Solarmer. SnO_2 colloid precursor was purchased from Alfa Aesar. Anhydrous dimethylformamide (DMF), isopropanol (IPA) and chlorobenzene (CB) were acquired from J&K. Chloroform (CF) was purchased from Sigma-Aldrich. All the chemicals were used as received without further treatment. The PbI_2·xDMAI complex was synthesized following our previous report.[44, 45] ZnO nanoparticles were synthesized according to previous report.[50] Generally, the solution of KOH (1.48 g in 65 mL methanol) was slowly dripped into the $Zn(Ac)_2·2H_2O$ solution (2.95g in 125 mL methanol) under vigorous stirring in 10 min. After 3 h, the heater and stirrer were stopped to allow the nanoparticles to precipitate for about 5 h. After separating the precipitate and mother liquor, the precipitate was washed twice with methanol. Then the suspension was unstirred for 5 h to reach complete precipitation. The washed precipitate was dispersed in IPA (10 mL) for further use.

3.2 Device fabrication

Solution Preparation: The SnO_2 solution was prepared by diluting the SnO_2 colloid precursor with deionized H_2O (v:v=1:5). $CsPbI_{2.1}Br_{0.9}$ solution was prepared by dissolving CsI (78 mg, 0.3 mmol), xDMAI·PbI_2 (105 mg, 0.165 mmol) and $PbBr_2$ (49.55 mg, 0.135 mmol) in 550 µL anhydrous DMF and stirred for 2 hours before use. $FA_{0.8}Cs_{0.2}Pb(I_{0.6}Br_{0.4})_3$ solution was prepared by dissolving FAI (148.52 mg, 0.864 mmol), CsI (56.16 mg, 0.216 mmol), PbI_2 (273.83 mg, 0.594 mmol) and $PbBr_2$ (178.36 mg,

0.486 mmol) in 360 µL anhydrous DMSO and 1080 µL anhydrous DMF. PMACl solution with different concentration was prepared by dissolving different weight of PMACl in IPA. For the HTL solution, 5 mg PBDB-T was dissolved in 1 mL anhydrous CB. OPV active layer solutions (PM6:Y6, 1:1.2) were prepared as our previous reports by dissolving 8 mg PM6 and 9.6 mg Y6 in 1 mL chloroform with 1% (vol%) 1-chloronaphthalene (CN) as additive.[54]

Single-junction perovskite device fabrication: ITO substrates were cleaned with detergent, deionized water, acetone, isopropanol and ethanol for 15 min, respectively. The cleaned ITO substrates were treated with UV ozone for 30 min before use. SnO_2 solution was spin-coated on ITO substrate at 5000 rpm for 30s and annealed at 150 °C for 30 min, then the substrates were transferred into a dry air glove box. 40 µL $CsPbI_{2.9}Br_{0.1}$ perovskite solution was spin-coated on the glass/ITO/SnO_2 substrate at 2000 rpm for 30 s and annealed at 170 °C for 10 min. Then, the glass/SnO_2/perovskite substrates were transferred into a N_2 glove box. PMACl with different concentration in IPA was spin-coated onto $CsPbI_{2.9}Br_{0.1}$ film at 6000 rpm for 30 s, followed by annealing at 100 °C for 5 min. Sequentially, IPA was spin-coated on the surface at 6000 rpm for 30 s, and annealed at 100 °C for another 5 min. To deposit the HTL, 20 µL PBDB-T solution was spin-coated on ITO/SnO_2/$CsPbI_{2.1}Br_{0.9}$/PMACl at 1500 rpm for 30s. Ultimately, 6 nm MoO_3 and 100 nm Ag were thermally evaporated.

Single-junction wide-bandgap: $FA_{0.8}Cs_{0.2}Pb(I_{0.6}Br_{0.4})_3$-based device fabrication. Glass/ITO/SnO_2 substrate was processed as the procedures mentioned above. After transferring the substrates into a N_2 glovebox, 40 µL $FA_{0.8}Cs_{0.2}Pb(I_{0.6}Br_{0.4})_3$ solution was spin coated on the Glass/ITO/SnO_2 substrate at 5000 rpm for 30 s. 200 µL CB was dripped onto film at 7 s before the end of spin-coating. Then PBDB-T, MoO_3 and Ag were deposited with the same procedures mentioned above.

Single Junction OSC Device Fabrication: ITO glass substrate was treated with the same procedures mentioned above, then the substrate was transferred to a N_2 glovebox. 30 nm ZnO film was deposited on the ITO by spin-coating the dispersion of ZnO in IPA. The active layer (PM6:Y6) solution was dynamically spin-coated onto the substrates at 2000 rpm for 60 s. Eventually, 10 nm MoO_3 and 100 nm Ag were thermally evaporated.

Tandem Device Fabrication: Glass/ITO/SnO_2 substrate was processed as the procedures mentioned above. Then the $CsPbI_{2.9}Br_{0.1}$ and $FA_{0.8}Cs_{0.2}Pb(I_{0.6}Br_{0.4})_3$ perovskite, PBDB-T were deposited by the procedures mentioned above respectively. Afterwards, 6 nm MoO_3 and 1 nm Ag were evaporated onto the PBDB-T layer. Then, 50 nm ZnO was spin-coated on the silver. Subsequentially, the PM6:Y6 active layer, MoO_3 (10 nm) and Ag (100 nm) were deposited with the same procedures mentioned above.

3.3 Characterization

J–V characteristics of single-junction and tandem devices were measured in N_2 glovebox using a Keithley 2400 source meter under simulated AM 1.5G illumination from a solar simulator (Enlitech, SS-F5, Taiwan). A National Renewable Energy Laboratory calibrated silicon solar cell with a KG2 filter was used to calibrate the intensity of light from solar simulator. EQE measurements were carried out by a QE-R EQE system (EnLi Technology, Taiwan), light bias with L700 filter (for the top cell) and S550 filter (for the bottom cell) were employed to measure the EQE of tandem devices. PL and TRPL results were recorded with a FLS980 spectrofluorometer (Edinburgh). The samples for PL and TRPL measurements were all formed on glass/ITO/SnO_2 substrate. UV–vis absorption spectra were measured with a UV–vis spectrometer (PerkinElmer model Lambda 2S). The thicknesses of films were measured by using a DektakXT Profiler (Bruker). The cross-section SEM image of tandem solar cells was monitored by scanning electron microscopy (SEM, Philips XL30 FEG). SP8) with a pulsed excitation laser at a wavelength of 405 nm.

3.4 Energy loss analysis.

The energy loss calculation follows previous work.[51, 52]

(1) The *Transmission Loss* was calculated as:

$$E_{trans}= \int_0^{Eg} \Phi(\boldsymbol{h\nu})\boldsymbol{dh\nu}$$

where Φ(hν) is solar energy spectrum. Eg is the band gap of solar cell system, and hν is the photon energy.

(2) *Insufficient Light Absorbing Loss* can be calculated as:

$$E_{abs}= \int_{Eg}^{4.43}\left(\mathbf{1}-\boldsymbol{EQE}(\mathbf{100\%}\boldsymbol{IQE},\boldsymbol{h\nu})\right)\Phi(\boldsymbol{h\nu})\boldsymbol{dh\nu}$$

where the EQE (100% IQE, hν) is the EQE of device assuming the device IQE is 100%, which can be estimated from the optical simulation and reflectance spectra.

(3) *Thermalization Energy Loss* can be calculated as:

$$E_{therm}= \int_{Eg}^{4.43}\left(\mathbf{1}-\frac{\boldsymbol{Eg}}{\boldsymbol{h\nu}}\right)\boldsymbol{EQE}(\boldsymbol{h\nu})\Phi(\boldsymbol{h\nu})\boldsymbol{dh\nu}$$

(4) V_{OC} loss can be calculated as:

$$E_{VOC}= \int_{Eg}^{4.43}[\frac{(\boldsymbol{Eg}-\boldsymbol{VOC})}{\boldsymbol{h\nu}}]\boldsymbol{EQE}(\boldsymbol{h\nu})\Phi(\boldsymbol{h\nu})\boldsymbol{dh\nu}$$

(5) *IQE loss* can be calculated as:

$$E_{IQE}= \int_{Eg}^{4.43}(\mathbf{1}-\boldsymbol{IQE}(\boldsymbol{h\nu}))\boldsymbol{EQE}(\mathbf{100\%}\boldsymbol{IQE},\boldsymbol{h\nu})\Phi(\boldsymbol{h\nu})\boldsymbol{dh\nu}$$

(6) FF loss can be calculated as:

$$E_{FF}=(1\text{-}FF)\left(\int_{Eg}^{4.43}\Phi(\boldsymbol{h\nu})\boldsymbol{dh\nu}\text{- }E_{trans}\text{- }E_{abs}\text{- }E_{therm}\text{- }E_{VOC}\text{- }E_{IQE}\right)$$

(7) Combining E_{abs} and E_{IQE}:

$$E_{abs}+E_{IQE}= \int_{Eg}^{4.43}\left(\mathbf{1}-\boldsymbol{EQE}(\boldsymbol{h\nu})\right)\Phi(\boldsymbol{h\nu})\boldsymbol{dh\nu}$$

Conclusions

We have successfully fabricated tandem solar cells with all-inorganic perovskite and organic absorbers for top and bottom sub cell respectively. Tandem devices with the passivated $CsPbI_{2.1}Br_{0.9}$ perovskite and narrow bandgap OSC active layer (PM6:Y6) have realized a remarkable PCE of 18.06 %, with V_{OC} of 1.89 V, J_{SC} of 12.77 mA cm^{-2}, and FF of 74.81 %. The all-inorganic perovskite $CsPbI_{2.1}Br_{0.9}$ showed superior

photostability to organic/inorganic hybrid perovskite $FA_{0.8}Cs_{0.2}Pb(I_{0.6}Br_{0.4})_3$, without phase segregation observed under one sun illumination. Therefore, the stable all-inorganic perovskite front cell can act as a windows layer to absorb high-energy UV light to protect the UV-unstable bottom organic solar cells. The tandem device showed excellent stability under one sun illumination, UV irradiation and 80 °C heat in N_2 atmosphere, respectively, in comparison, organic/inorganic hybrid perovskite-based tandem device exhibited obvious degradation. In conclude, we have systematically studied the stability and performance issue of all-inorganic perovskite/organic tandem solar cells, which proves that all-inorganic perovskites are more promising candidates than organic-inorganic hybrid perovskites for the fabrication of efficient and stable tandem solar cells.

Author Contributions

X. Wu conceived the ideas, designed the experiments, fabricated, and characterized devices, analysed data, conducted the calculations of energy loss, wrote original draft, draft and finalized the manuscript. Y Liu helped to write, draft and finalized the manuscript. F. Qi synthesized the ZnO NPs and $DMAI{\cdot}PbI_2$ complex and revised the manuscript. F. Lin helped to design the experiments and revised the manuscript. H. Fu and K. Jiang helped to design the experiments of organic solar cells and analyse data. S. Wu, L. Bi, D. Wang helped to analysed data of PL, TRPL, Absorption and stability. F. Xu revised the manuscript. Z. Zhu and Alex K.-Y Jen supervised the project and revised the paper.

Conflicts of interest

There are no conflicts to declare.

Acknowledgements

This work was supported by the APRC Grant of the City University of Hong Kong (9610421), Innovation and Technology Fund (ITS/497/18FP, GHP/021/18SZ), the Office of Naval Research (N00014-17-1-2201), National Science Foundation (DMR-1608279), the Air Force Office of Scientific Research (FA9550-18-1-0046), the ECS grant (CityU 21301319) from the Research Grants Council of Hong Kong, Natural Science Foundation of Guangdong Province (2019A1515010761), Guangdong Major Project of Basic and Applied Basic Research (No. 2019B030302007), Guangdong-Hong Kong-Macao joint laboratory of optoelectronic and magnetic functional materials (No. 2019B121205002), the National Natural Science Foundation of China (No. 62001308), Research Grants for Universities in Guangdong Province through Innovative Project for Young Talents (No. 2018KQNCX398).

References

1. M. A. Green, E. D. Dunlop, J. Hohl‐Ebinger, M. Yoshita, N. Kopidakis and X. Hao, *Progress in Photovoltaics: Research and Applications*, 2020, **28**, 629-638.
2. X. Zheng, Y. Hou, C. Bao, J. Yin, F. Yuan, Z. Huang, K. Song, J. Liu, J. Troughton and N. Gasparini, *Nat. Energy*, 2020, **5**, 131-140.
3. Q. Jiang, Y. Zhao, X. Zhang, X. Yang, Y. Chen, Z. Chu, Q. Ye, X. Li, Z. Yin and J. You, *Nat. Photonics*, 2019, **13**, 460-466.
4. G. Kim, H. Min, K. S. Lee, S. M. Yoon and S. I. Seok, *Science*, 2020, **370**, 108-112.
5. M. Jeong, I. W. Choi, E. M. Go, Y. Cho, M. Kim, B. Lee, S. Jeong, Y. Jo, H. W. Choi and J. Lee, *Science*, 2020, **369**, 1615-1620.
6. A. Rajagopal, K. Yao and A. K. Y. Jen, *Adv. Mater.*, 2018, **30**, 1800455.
7. S. Rühle, *Sol. Energy*, 2016, **130**, 139-147.
8. K. Yoshikawa, H. Kawasaki, W. Yoshida, T. Irie, K. Konishi, K. Nakano, T. Uto, D. Adachi, M. Kanematsu, H. Uzu and K. Yamamoto, *Nat. Energy*, 2017, **2**, 17032.
9. G. E. Eperon, M. T. Hörantner and H. J. Snaith, *Nature Reviews Chemistry*, 2017, **1**, 1-18.
10. T. Leijtens, K. A. Bush, R. Prasanna and M. D. McGehee, *Nat. Energy*, 2018, **3**, 828-838.
11. Y. Hou, E. Aydin, M. De Bastiani, C. Xiao, F. H. Isikgor, D.-J. Xue, B. Chen, H. Chen, B. Bahrami and A. H. Chowdhury, *Science*, 2020, **367**, 1135-1140.
12. J. Xu, C. C. Boyd, J. Y. Zhengshan, A. F. Palmstrom, D. J. Witter, B. W. Larson, R. M. France, J. Werner, S. P. Harvey and E. J. Wolf, *Science*, 2020, **367**, 1097-1104.
13. D. H. Kim, C. P. Muzzillo, J. Tong, A. F. Palmstrom, B. W. Larson, C. Choi, S. P. Harvey, S. Glynn, J. B. Whitaker and F. Zhang, *Joule*, 2019, **3**, 1734-1745.
14. Q. Han, Y.-T. Hsieh, L. Meng, J.-L. Wu, P. Sun, E.-P. Yao, S.-Y. Chang, S.-H. Bae, T. Kato and V. Bermudez, *Science*, 2018, **361**, 904-908.
15. Z. Li, Y. Zhao, X. Wang, Y. Sun, Z. Zhao, Y. Li, H. Zhou and Q. Chen, *Joule*, 2018, **2**, 1559-1572.
16. L. Mazzarella, Y. H. Lin, S. Kirner, A. B. Morales‐Vilches, L. Korte, S. Albrecht, E. Crossland, B. Stannowski, C. Case, H. J. Snaith and R. Schlatmann, *Adv. Energy Mater.*, 2019, **9**, 1803241.
17. A. F. Palmstrom, G. E. Eperon, T. Leijtens, R. Prasanna, S. N. Habisreutinger, W. Nemeth, E. A. Gaulding, S. P. Dunfield, M. Reese and S. Nanayakkara, *Joule*, 2019, **3**, 2193-2204.
18. D. P. McMeekin, G. Sadoughi, W. Rehman, G. E. Eperon, M. Saliba, M. T. Hörantner, A. Haghighirad, N. Sakai, L. Korte and B. Rech, *Science*, 2016, **351**, 151-155.
19. R. Lin, K. Xiao, Z. Qin, Q. Han, C. Zhang, M. Wei, M. I. Saidaminov, Y. Gao, J. Xu and M. Xiao, *Nat. Energy*, 2019, **4**, 864-873.
20. K. Xiao, R. Lin, Q. Han, Y. Hou, Z. Qin, H. T. Nguyen, J. Wen, M. Wei, V. Yeddu, M. I. Saidaminov, Y. Gao, X. Luo, Y. Wang, H. Gao, C. Zhang, J. Xu, J. Zhu, E. H. Sargent and H. Tan, *Nat. Energy*, 2020, DOI: 10.1038/s41560-020-00705-5.
21. Z. Yang, Z. Yu, H. Wei, X. Xiao, Z. Ni, B. Chen, Y. Deng, S. N. Habisreutinger, X. Chen, K. Wang, J. Zhao, P. N. Rudd, J. J. Berry, M. C. Beard and J. Huang, *Nat. Commun.*, 2019, **10**, 4498.
22. D. Zhao, C. Chen, C. Wang, M. M. Junda, Z. Song, C. R. Grice, Y. Yu, C. Li, B. Subedi and N. J. Podraza, *Nat. Energy*, 2018, **3**, 1093-1100.

23. J. Tong, Z. Song, D. H. Kim, X. Chen, C. Chen, A. F. Palmstrom, P. F. Ndione, M. O. Reese, S. P. Dunfield and O. G. Reid, *Science*, 2019, **364**, 475-479.
24. C. Li, Y. Wang and W. C. Choy, *Small Methods*, 2020, 2000093.
25. C.-Y. Chang, B.-C. Tsai, Y.-C. Hsiao, M.-Z. Lin and H.-F. Meng, *Nano Energy*, 2019, **55**, 354-367.
26. P. Cheng, Y. Liu, S.-Y. Chang, T. Li, P. Sun, R. Wang, H.-W. Cheng, T. Huang, L. Meng and S. Nuryyeva, *Joule*, 2019, **3**, 432-442.
27. L. Zuo, J. Yu, X. Shi, F. Lin, W. Tang and A. K. Y. Jen, *Adv. Mater.*, 2017, **29**, 1702547.
28. L. Zuo, C. C. Chueh, Y. X. Xu, K. S. Chen, Y. Zang, C. Z. Li, H. Chen and A. K. Y. Jen, *Adv. Mater.*, 2014, **26**, 6778-6784.
29. L. Meng, Y. Zhang, X. Wan, C. Li, X. Zhang, Y. Wang, X. Ke, Z. Xiao, L. Ding and R. Xia, *Science*, 2018, **361**, 1094-1098.
30. G. Liu, J. Jia, K. Zhang, X. e. Jia, Q. Yin, W. Zhong, L. Li, F. Huang and Y. Cao, *Adv. Energy Mater.*, 2019, **9**, 1803657.
31. Y. An, X. Liao, L. Chen, J. Yin, Q. Ai, Q. Xie, B. Huang, F. Liu, A. K. Y. Jen and Y. Chen, *Adv. Funct. Mater.*, 2018, **28**, 1706517.
32. Z. Li, S. Wu, J. Zhang, K. C. Lee, H. Lei, F. Lin, Z. Wang, Z. Zhu and A. K. Jen, *Adv. Energy Mater.*, 2020, **10**, 2000361.
33. Q. Zeng, L. Liu, Z. Xiao, F. Liu, Y. Hua, Y. Yuan and L. Ding, *Sci Bull*, 2019, **64**, 885.
34. J. Liu, S. Lu, L. Zhu, X. Li and W. C. Choy, *Nanoscale*, 2016, **8**, 3638-3646.
35. A. Rajagopal, R. J. Stoddard, S. B. Jo, H. W. Hillhouse and A. K.-Y. Jen, *Nano Lett.*, 2018, **18**, 3985-3993.
36. R. J. Stoddard, A. Rajagopal, R. L. Palmer, I. L. Braly, A. K.-Y. Jen and H. W. Hillhouse, *ACS Energy Lett.*, 2018, **3**, 1261-1268.
37. A. Rajagopal, Z. Yang, S. B. Jo, I. L. Braly, P. W. Liang, H. W. Hillhouse and A. K. Y. Jen, *Adv. Mater.*, 2017, **29**, 1702140.
38. W. Chen, J. Zhang, G. Xu, R. Xue, Y. Li, Y. Zhou, J. Hou and Y. Li, *Adv. Mater.*, 2018, **30**, e1800855.
39. F. Bai, J. Zhang, Y. Yuan, H. Liu, X. Li, C. C. Chueh, H. Yan, Z. Zhu and A. K. Y. Jen, *Adv. Mater.*, 2019, **31**, 1904735.
40. P. Wang, Y. Zhao and T. Wang, *Appl. Phys. Rev.*, 2020, **7**, 031303.
41. H. Aqoma, I. F. Imran, F. T. A. Wibowo, N. V. Krishna, W. Lee, A. K. Sarker, D. Y. Ryu and S. Y. Jang, *Adv. Energy Mater.*, 2020, **10**, 2001188.
42. K. Lang, Q. Guo, Z. He, Y. Bai, J. Yao, M. Wakeel, M. S. Alhodaly, T. Hayat and Z. a. Tan, *J. Phys. Chem. Lett.*, 2020, **11**, 9596-9604.
43. S. Xie, R. Xia, Z. Chen, J. Tian, L. Yan, M. Ren, Z. Li, G. Zhang, Q. Xue and H.-L. Yip, *Nano Energy*, 2020, **78**, 105238.
44. T. Liu, J. Zhang, X. Wu, H. Liu, F. Li, X. Deng, F. Lin, X. Li, Z. Zhu and A. K.-Y. Jen, *Solar RRL*, 2000205.
45. X. Wu, F. Qi, F. Li, X. Deng, Z. Li, S. Wu, T. Liu, Y. Liu, J. Zhang and Z. Zhu, *Energy & Environmental Materials,*, **DOI:10.1002/eem2.12089**.
46. F. Qi, X. Deng, X. Wu, L. Huo, Y. Xiao, X. Lu, Z. Zhu and A. K. Y. Jen, *Adv. Energy Mater.*, 2019, **9**, 1902600.
47. J. Wang, J. Zhang, Y. Zhou, H. Liu, Q. Xue, X. Li, C.-C. Chueh, H.-L. Yip, Z. Zhu and A. K. Jen, *Nat. Commun.*, 2020, **11**, 177.
48. M. Abdi-Jalebi, Z. Andaji-Garmaroudi, S. Cacovich, C. Stavrakas, B. Philippe, J. M. Richter, M. Alsari, E. P. Booker, E. M. Hutter, A. J. Pearson, S. Lilliu, T. J. Savenije, H. Rensmo, G. Divitini, C. Ducati, R. H. Friend and S. D. Stranks, *Nature*, 2018, **555**, 497-501.
49. M. Yuan, L. N. Quan, R. Comin, G. Walters, R. Sabatini, O. Voznyy, S. Hoogland, Y. Zhao, E. M. Beauregard and P. Kanjanaboos, *Nat. Nanotechnol.*, 2016, **11**, 872-877.
50. W. J. Beek, M. M. Wienk, M. Kemerink, X. Yang and R. A. Janssen, *The Journal of Physical Chemistry B*, 2005, **109**, 9505-9516.
51. L. Zuo, X. Shi, S. B. Jo, Y. Liu, F. Lin and A. K. Y. Jen, *Adv. Mater.*, 2018, **30**, 1706816.
52. L. Zuo, X. Shi, W. Fu and A. K. Y. Jen, *Adv. Mater.*, 2019, **31**, 1901683.
53. J. Jeong, J. Seo, S. Nam, H. Han, H. Kim, T. D. Anthopoulos, D. D. Bradley and Y. Kim, *Adv. Sci.*, 2016, **3**, 1500269.
54. H. Fu, W. Gao, Y. Li, F. Lin, X. Wu, J. H. Son, J. Luo, H. Y. Woo, Z. Zhu and A. K. Y. Jen, *Small Methods*, 2020, 2000687.